

Signatures of the superfluid to Mott insulator transition in cold bosonic atoms in a one dimensional optical lattice

S. Ramanan*

Centre for High Energy Physics, Indian Institute of Science, Bangalore 560012, India

Tapan Mishra[†] and Meetu Sethi Luthra[‡]

Indian Institute of Astrophysics, II Block, Kormangala, Bangalore, 560 034, India.

Ramesh V. Pai[§]

Department of Physics, Goa University, Taleigao Plateau, Goa 403 206, India.

B. P. Das[¶]

Indian Institute of Astrophysics, II Block, Kormangala, Bangalore, 560 034, India.

(Dated: August 22, 2018)

We study the Bose-Hubbard model using the finite size density matrix renormalization group method. We obtain for the first time a complete phase diagram for a system in the presence of a harmonic trap and compare it with that of the homogeneous system. To realize the transition from the superfluid to the Mott insulator phase we investigate different experimental signatures of these phases in quantities such as momentum distribution, visibility, condensate fraction and the total number of bosons at a particular density. The relationships between the various experimental signatures and the phase diagram are highlighted.

PACS numbers: 03.75.Nt, 05.10.Cc, 05.30.Jp, 73.43.Nq

I. INTRODUCTION

In recent years many theoretical and experimental investigations have been carried out in the field of ultra-cold atoms in optical lattices [1, 2, 3]. The interest in bosonic systems began with the seminal paper by Fisher *et al* [4], where a phase transition from a superfluid (SF) to a Mott insulator (MI) in a lattice of bosons was predicted when the on-site Coulomb repulsion between the atoms dominates the nearest neighbor hopping amplitude. Since then, a variety of theoretical approaches [5, 6, 7, 8, 9, 10, 11, 12, 13, 14, 15] have been used to study the Bose-Hubbard Model (BHM) [4]. There is good agreement between the phase diagrams obtained from the different techniques. While the BHM was originally developed in the context of ⁴He [4], its potential to describe ultra cold bosons trapped in an optical lattice was soon realized by Jaksch *et al* [16]. This paper has had a great impact on the condensed matter community because high-precision experiments on cold atoms in traps can now be used as a powerful and reliable tool to study a variety of quantum phase transitions [1, 2, 3]. The experimental realization of the quantum phase tran-

sition from the superfluid to the Mott insulator in three dimensions [17], two dimensions [18], as well as in one dimension [19] soon followed. The bosons in an optical lattice are well described by the Bose-Hubbard model modified to include a trap potential [16], which is normally harmonic. In the presence of a trap, the density profile exhibits a rich structure as the SF and the MI phases co-exist. A variety of numerical methods have been applied to understand the model [20, 21, 22, 23, 24, 25, 26]. The most important aspect that has emerged is the lack of a global phase in these systems. As an analogy, in three dimensions the superfluid and the Mott insulator phases coexist as shells in an onion. The unprecedented control over the system parameters by tuning the laser intensity has paved the path for the experimental realization of these predictions [27, 28].

In this paper, we re-visit the one dimensional Bose-Hubbard model using the density matrix renormalization group method. Our main motivation is to obtain the phase diagram, given the experimental realization of the shell structure and their signatures. The Bose-Hubbard model, describing bosons in an optical lattice, is given by

$$H = -t \sum_{\langle i,j \rangle} (a_i^\dagger a_j + h.c) + \frac{U}{2} \sum_i n_i(n_i - 1) + V_t \sum_i r_i^2 n_i. \quad (1)$$

where t is the hopping amplitude, U is the on-site repulsion between the atoms and V_t is the depth of the external trapping potential, a_i^\dagger (a_i) are the bosonic creation (annihilation) operator, $n_i = a_i^\dagger a_i$ is the number operator and r_i is the position of the i^{th} lattice site from

*Electronic address: suna@cts.iisc.ernet.in

[†]Electronic address: tapan@iiap.res.in

[‡]Electronic address: sethi.meetu@gmail.com; permanent address Bhaskaracharya College of Applied Sciences, Phase-I, Sector-2, Dwarka, Delhi, 110075, India.

[§]Electronic address: rvpai@unigoa.ac.in

[¶]Electronic address: das@iiap.res.in

the trap center. For simplicity, the energy is scaled in units of the hopping amplitude which is set to one.

In experiments, the optical lattice potential (V_{OL}), formed by the superposition of three counter propagating laser beams [2, 29], can be written as:

$$V_{OL} = V_0(\sin^2(k_L x) + \sin^2(k_L y) + \sin^2(k_L z)) \quad (2)$$

where V_0 is the lattice depth measured in units of the single photon recoil energy E_R , $k_L = 2\pi/\lambda_L$ is the wave vector and λ_L is the laser wavelength. By increasing the intensity of the beam in two directions, the hopping is restricted to one dimension and this results in a one dimensional lattice. The on-site interaction U and the hopping amplitude t are related to V_0 and E_R as follows:

$$\frac{U}{t} \propto \exp(2V_0/E_R)^{1/2}. \quad (3)$$

Therefore, by varying the lattice depth the ratio of U/t can be tuned.

Earlier studies of the homogeneous system show that when the on-site interaction strength U is small compared to the hopping amplitude t , the system remains in the SF phase characterized by long range coherence. When U increases and becomes much larger than t , a transition from the SF to the MI phase occurs at some critical value of $U = U_c \sim 3.4$ (in units of t) [8, 9, 10]. This transition belongs to the Kosterlitz-Thouless universality class [30, 31]. The SF-MI transition gets more interesting in the presence of a trap [32, 33, 34, 35]. In this case, the entire system remains in the SF phase for small U values, but as U increases, a MI phase develops around a central SF phase, followed by a SF shoulder. Further increase in U ultimately results in a MI phase throughout the lattice with the exception of the trap edges, which we refer to as a central MI phase. This alternating occurrence of the SF and the MI phases can be observed in the number density profile. The system exhibits a plateau at integer densities (MI phase) surrounded by a region of non-integer densities (SF phase) [20, 21, 22, 23, 24, 25, 26, 32, 33, 34, 35] and this has been recently observed in experiments [27, 28] in 3D optical lattices.

In this paper, we first obtain the phase diagram of the model, given by eqn. (1), in the homogeneous ($V_t = 0$) limit. We then extend our analysis to the inhomogeneous case and compare it with the homogeneous case. Finally we obtain experimentally measurable quantities like condensate fraction, visibility and density profile and deduce the inhomogeneous phase diagram. We also discuss how the shell structure in the optical lattice can be observed from condensate fraction and visibility.

This paper is structured as follows: Section (II) contains a brief discussion on the Finite Size Density Matrix Renormalization Group technique (FS-DMRG). Section (III) discusses the phase diagram obtained from the number density profile, while Section (IV) analyzes the experimental signature for the phase transition and we summarize our results in Section (V).

II. METHOD OF CALCULATION

We have employed the finite size density matrix renormalization group method (FS-DMRG) [36, 37] with open-boundary condition to determine the ground state energy and the wave function of the system. This method is one of the most powerful technique in one dimension and has been widely used to study the Bose-Hubbard model [8, 9, 10, 33, 34]. We have considered a soft-core case by retaining four bosonic states per site and the weight of the states neglected in the density matrix formed from the left or right blocks is less than 10^{-6} . For better convergence of the ground state energies of various phases, we have performed a finite size sweeping procedure [9, 36], twice in each iteration of the FS-DMRG method.

Our FS-DMRG method consists of two steps: (i) a DMRG iteration where the length of the system L is increased to $L + 2$ and (ii) finite size sweeping to achieve better convergence of the ground state energy $E_L(N)$ [9, 36]. We consider a system with an initial length $L = 4$ and the number of bosons $N = 4$. The FS-DMRG procedure is then employed, keeping the density of bosons fixed at $\rho = 1$, until we have a desired number of bosons in the system, say $N = 30$. Then onwards, in the FS-DMRG iteration, only the length of the system is increased keeping N fixed, until the system grows to a desired size, for example $L = 100$. At this point we have a system of length $L = 100$ with $N = 30$ bosons. Now keeping the length fixed, we increase N in steps of 1 at the end of each FS-DMRG sweep. In our example, N is varied from 30 to 150. Thus at the end of the FS-DMRG calculation, for a given set of parameter values, we have ground state energies $E_L(N)$ and wave functions $|\psi_{LN}\rangle$ for a system of length $L = 100$ with N varying from 30 to 150. From $E_L(N)$, we obtain the chemical potential μ of the system

$$\mu = \frac{\delta E_L(N)}{\delta N}. \quad (4)$$

The on-site local number density $\langle n_i \rangle$ and the local compressibility κ_i are defined as

$$\langle n_i \rangle = \langle \psi_{LN} | n_i | \psi_{LN} \rangle \quad (5)$$

$$\kappa_i = \frac{\delta n_i}{\delta \mu}. \quad (6)$$

For the homogeneous case, the local density $\langle n_i \rangle = N/L$ and hence the compressibility are uniform throughout the system except at the edges due to boundary effects. The chemical potential corresponds to that of the whole system. However, for finite V_t the lattice is inhomogeneous and as a result the local density $\langle n_i \rangle$ attains its maximum value at the center of the trap where the potential is minimum and decreases as we move away from the center, eventually going to zero.

In most of our calculations, we have taken $V_t = 0.004$ and 0.008 , $L = 200$, with N ranging between 30 and 150 and U between 2 and 20.

III. RESULTS AND DISCUSSIONS

A. Homogeneous case

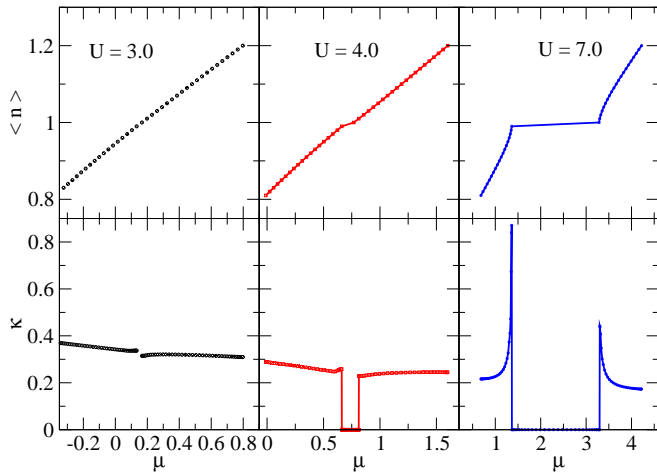


FIG. 1: Variation of the compressibility κ (lower panels) and the density $\langle n \rangle$ (upper panels) as a function of μ for the homogeneous case ($V_t = 0$). The plateau region at $\langle n \rangle = 1$ and $\kappa = 0$ signals the incompressible ($\rho = 1$) MI phase.

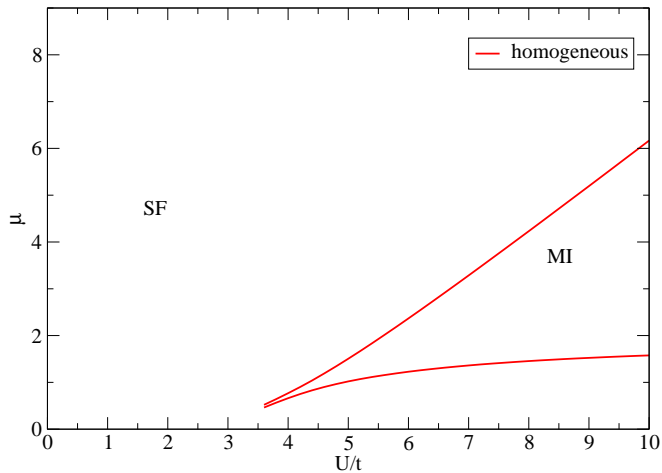


FIG. 2: Phase diagram for the homogeneous Bose-Hubbard model. The MI phase has density $\rho = 1$.

We begin our discussions with the homogeneous case. The density of the system $\langle n \rangle$ as a function of the chemical potential μ for three values of $U = 3, 4$ and 7 are shown in the top panels of Fig. (1). The formation of a plateau in the $\langle n \rangle$ versus μ plots, for $U = 4$ and 7 at

$\langle n \rangle = 1$, in contrast to $U = 3$, signals the onset of the $\rho = 1$ MI phase, where ρ denotes the density per site. The lower panels in Fig. (1) show the compressibility κ (calculated using Eq. (6)) as a function of μ . It is clear that the MI phase is incompressible, i.e., $\kappa = 0$. The cusp in κ as $\langle n \rangle$ approaches 1, shown in Fig. (1), is due to quantum criticality. The phase diagram for the homogeneous system is obtained by picking out the values of μ at the knees where $\langle n \rangle = 1$ and $\kappa = 0$ and plotting them in the $\mu - U$ plane. This is shown in the fig. (2) and is in agreement with earlier results [8, 9, 10, 13]. The cusp in the compressibility reflects the Kosterlitz-Thouless type behavior of the SF-MI transition.

B. Inhomogeneous case

We now analyze the case when there is a finite trapping potential V_t in the Bose-Hubbard Hamiltonian. Taking the depth of the trap $V_t = 0.004$, number of bosons $N = 100$ and length $L = 200$, we obtain the local density profile $\langle n_i \rangle$ as a function of the distance from the center of the trap r_i , as shown in Fig. (3). In contrast to the homogeneous case, $\langle n_i \rangle$ is not uniform when the trap is finite. It decreases monotonically as we move from the center of the trap towards the edges. For larger values of U ($U > 6$) the density profile develops a well defined plateau at $\langle n_i \rangle = 1$ and the length of the plateau grows as U is increased further. A simple way to understand the behavior of $\langle n_i \rangle$ is through the Local Density Approximation (LDA) [23, 35] where the local density at site i in the trapped case is given by the density of a homogeneous system with a chemical potential

$$\mu_i = \mu - V_t r_i^2. \quad (7)$$

Here μ refers to the chemical potential at the center of the lattice where the trap potential is zero. Using Eq. (7) we can re-scale the x-axis of Fig. (3), so that we get the local density as a function of the local chemical potential, as shown in Fig. (4) for $U = 3$ and 9 , where the homogeneous case is also documented for comparison. The local density as a function of the local chemical potential exhibits trends similar to the homogeneous system, that is the value of $\langle n_i \rangle$ increases smoothly as μ_i increases for lower values of U , where the entire system is in the compressible superfluid phase. However, as U increases further, a clear plateau emerges at $\langle n_i \rangle = 1$ indicating the onset of the $\rho = 1$ MI phase.

The local compressibility can be obtained from the local density using eqn. (6). Fig. (5) shows the local density and the local compressibility in the upper and the lower panels, respectively. The plateau region at $\langle n_i \rangle = 1$ (upper panels) has the corresponding local compressibility equal to zero. This verifies that the plateau present in the number density profile represents the MI phase. Furthermore, this confirms the coexistence of the SF and the MI phases in the presence of a trap. Though there is an overall agreement between the homogeneous and

the inhomogeneous cases, we note that there are slight discrepancies. The sharp SF-MI transition observed in the homogeneous system is smoothed out in the presence of a trap. The cusp like behavior observed in κ for the homogeneous case is also lost. The agreement between the homogeneous and the inhomogeneous cases prompted us to obtain the phase diagram for the inhomogeneous system, by analogously picking out the values of μ at the knees where $\langle n_i \rangle = 1$, and plotting them in the $\mu - U$ plane. The resultant phase diagram is compared with the homogeneous result in Fig. (6). It is interesting to note that the MI lobe for the inhomogeneous system lies within that of the homogeneous system. However, the MI lobe retains its cusp like shape. Thus the SF-MI transition for density $\rho = 1$ and $V_t > 0$ does have the Kosterlitz-Thouless universality class behavior.

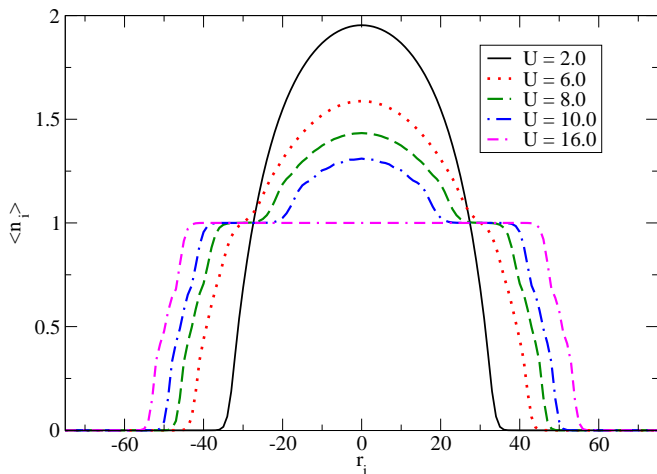


FIG. 3: Density profile as a function of r_i for $V_t = 0.004$, $L = 200$ and $N = 100$ for a range of U . Note that as the on-site repulsion increases, a MI phase forms around the central SF phase, finally leading to a central MI phase for higher values of U .

IV. EXPERIMENTAL SIGNATURES

In the earlier section we have established that the ground state phases for the Bose-Hubbard Hamiltonian given by eqn. (1) are either the superfluid or the Mott insulator depending on the ratio of U/t and the local chemical potential μ_i . Since μ_i is uniform for the homogeneous system, the ground state is global in nature. However, for inhomogeneous systems, μ_i being non uniform, both the SF and the MI phases coexist, as already discussed. It would be worthwhile to explore the signatures of these coexisting phases in experimentally determined quantities.

It is now possible in experiments to record the spatial distribution of the lattice with different filling factors using spatially selective microwave transitions and

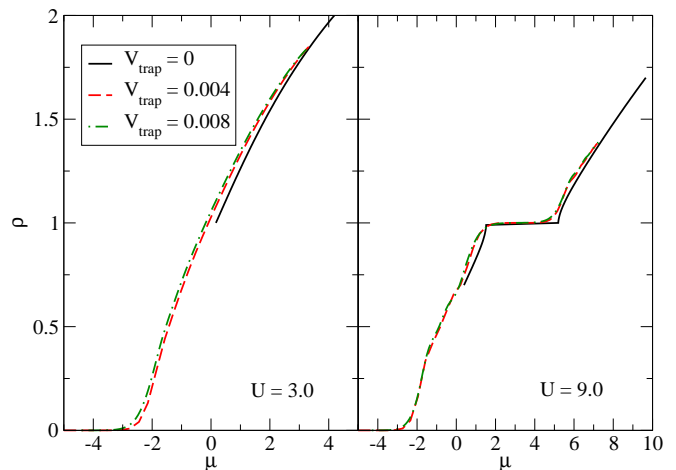


FIG. 4: Density as a function of chemical potential for the homogeneous and inhomogeneous cases. The solid line represents the homogeneous system, the dashed lines and dash-dot lines, the inhomogeneous case ($V_t = 0.004$ and $V_t = 0.008$ respectively). The homogeneous case has sharp transitions compared to the finite trap case.

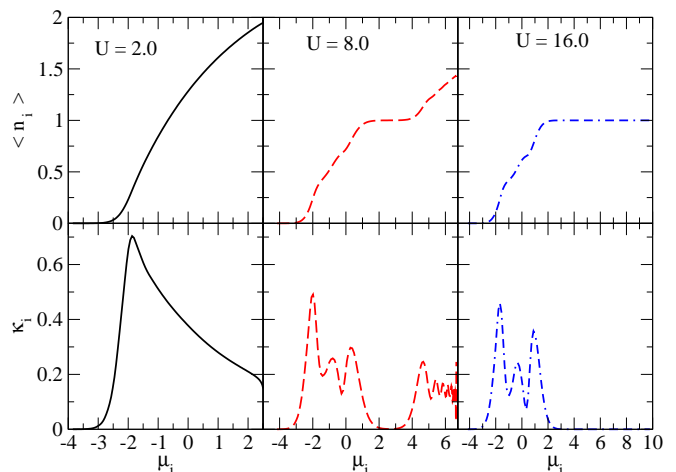


FIG. 5: Local density and local compressibility as a function of the local chemical potential for $V_t = 0.004$.

spin-changing collisions as shown by Fölling et al. [27]. Similar experiments in one-dimensional optical lattices can yield density profiles from which the phase diagram can be obtained, as discussed in the previous section. Another way to obtain direct information about the Mott plateaus (shells in 3D) is through the atomic clock shift experiment [28]. By using density dependent transition frequency shifts, sites with different occupation can be spectroscopically distinguished, thus giving us the information about the number of sites with a given density ρ , defined as $N(\rho)$. In Fig. (7) we plot $N(\rho)$ versus ρ for several values of U for a system with $V_t = 0.004$ and $N = 100$. The peak in $N(\rho)$ at $\rho = 1$ for $U > 6.0$ is a di-

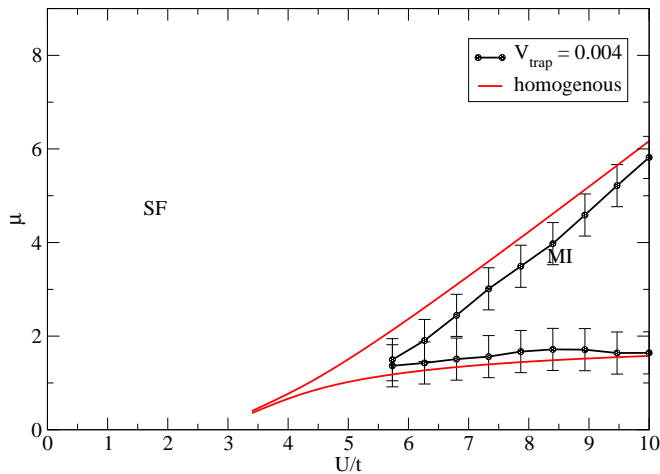


FIG. 6: Homogeneous and inhomogeneous phase diagram

rect signature of a well developed Mott insulator plateau in the inhomogeneous system. The size of this peak increases with U and is consistent with the increase in the length of the MI plateau as shown in the phase diagram (see Fig. (6)). From $N(\rho)$ we obtain the following quantities: N_{MI}/N , the fraction of number of bosons in the Mott plateau and N_{SF}/N , the fraction of bosons in the SF region. Here N_{MI} and N_{SF} are the number of bosons in the MI and the SF phases respectively. Fig. (8) shows both N_{MI}/N and N_{SF}/N for several values of U keeping $V_t = 0.004$. For $U < 6.0$, we observe that N_{SF}/N is close to one, while N_{MI}/N is close to zero. This is because the entire system is in the SF phase. However, for $U > 6.0$, the increase in N_{MI}/N , signals the formation of a MI plateau in the system. The critical value of U , marking the transition to the MI phase ($\rho = 1$) can be read-off from Fig. (8) and is given by $U_C \sim 6$. The small plateaus seen in N_{MI}/N and N_{SF}/N are indicative of the detailed distribution of the bosons as U increases in the presence of a trap.

In other experiments, the cold atom gas trapped in an optical lattice is allowed to expand and the interference pattern in the density of the expanding gas is recorded. The density distribution is mirrored in the momentum distribution defined as,

$$n(q) = \frac{1}{L} \sum_{k,l=1}^L \langle a_k^\dagger a_l \rangle \exp(iq(k-l)) \quad (8)$$

where k, l are the lattice sites. Fig. (9) shows the momentum distribution for different U values. The superfluid phase that has long-range coherence exhibits sharp interference peaks, while the Mott insulator phase, where the local density is pinned to integer values per site, breaks this coherence and hence no sharp peaks are observed [17]. Although the presence of the interference peaks in the density distribution (or analogously momentum distribution) was originally used to signal the forma-

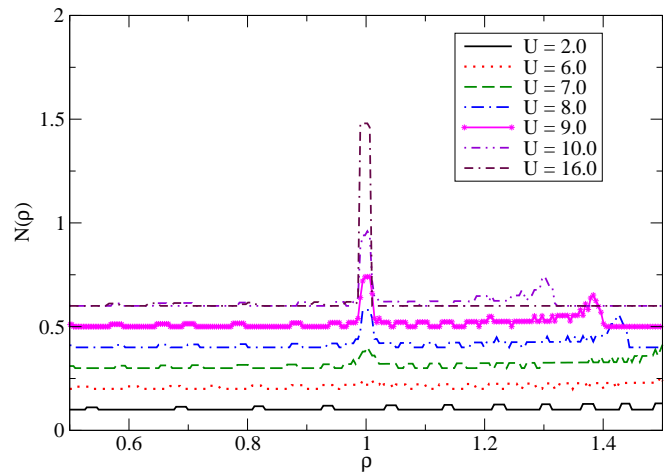


FIG. 7: $N(\rho)$ versus ρ for $V_t = 0.004$. A small offset is added to the Y-axis for clarity. The peak in $N(\rho)$ at $\rho = 1$ signals the MI plateau in density profile (Fig. 3) and thus confirms the coexistence of SF and MI phases.

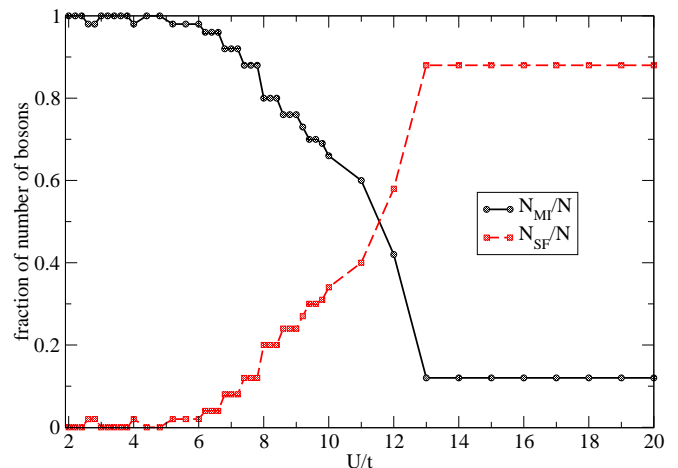


FIG. 8: N_{MI}/N and N_{SF}/N as function of U . The critical on-site interaction $U_C \sim 6.0$ for the SF-MI transition for $\rho = 1$ can be easily read-off.

tion of a SF phase, recently it has been established that the visibility of the interference fringes [29, 38, 39, 40] provides a clear signature of the transition. The fringe visibility is defined as

$$\mathcal{V} = \frac{N_{\text{max}} - N_{\text{min}}}{N_{\text{max}} + N_{\text{min}}} \quad (9)$$

where N_{max} and N_{min} are the maximum and the minimum of the momentum distribution measured at $q = \pm 2\pi$ and $q = \pm \pi$ respectively, in one dimension. The condensate fraction, that is the number of bosons in the condensate with respect to the total number of bosons, is defined as the largest eigenvalue of the matrix $\langle a_i^\dagger a_j \rangle$ divided by the total number of bosons [42]. The fringe

visibility and the corresponding condensate fraction for $V_t = 0.004$, $N = 100$ and $V_t = 0.008$, $N = 50$ are given in Figs. (10) and (11), respectively.

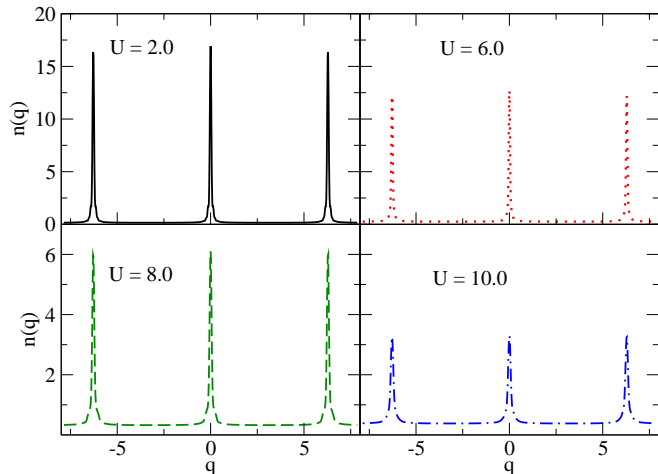


FIG. 9: Momentum distribution as a function of q in units of the lattice spacing. Note that at smaller U values there are three prominent interference peaks at $q = 0$ and $q = \pm 2\pi$. As U increases, the peaks get smaller, indicating a transition from SF to MI.

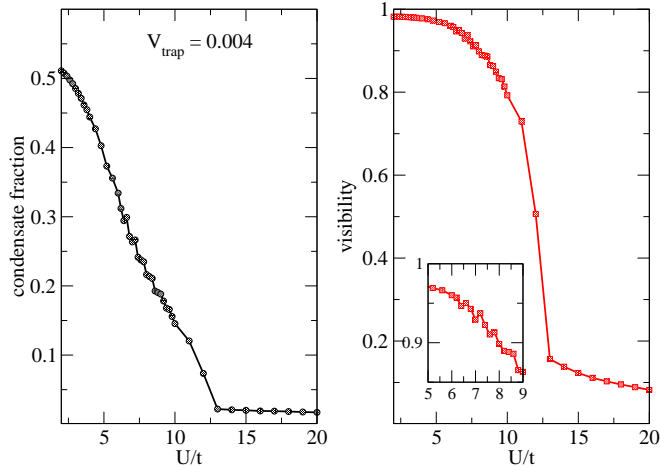


FIG. 10: Condensate fraction (left) and visibility (right) as a function of U for a trap of depth $V_t = 0.004$. The inset zooms in on the kinks observed in the visibility corresponding to the formation of Mott shoulders.

For a system in uniform SF phase, the fringe visibility is 1 [39]. In the homogeneous case, when the system undergoes a quantum phase transition from SF to MI, the visibility falls monotonously [29, 41]. In the presence of a trap, however, the visibility as a function of U has a rich structure due to the formation of alternating SF and MI shells [38]. From Figs. (10) and (11), we note the following for the trap case: (1) the visibility remains finite even at high U values (i.e., deep inside the MI lobes) compared

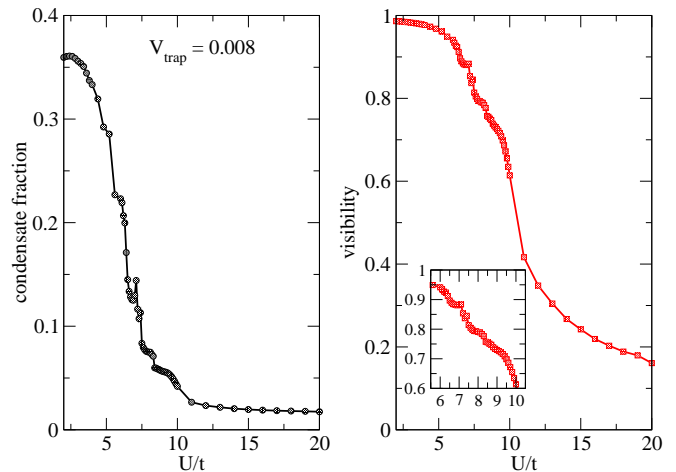


FIG. 11: Condensate fraction (left) and visibility (right) as a function of U for a trap of depth $V_t = 0.008$.

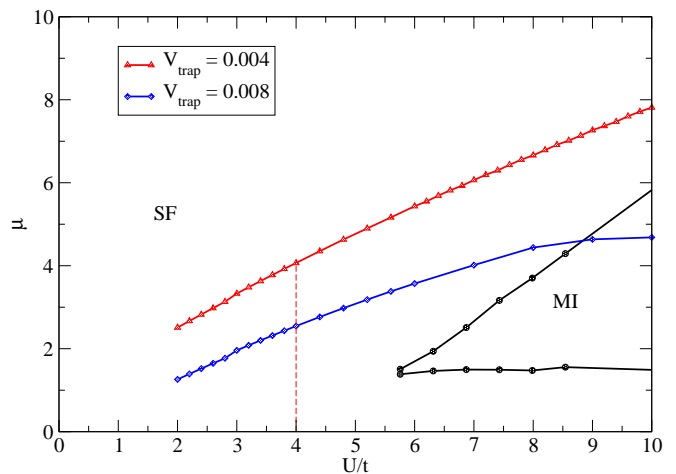


FIG. 12: Variation of μ_0 , the local chemical potential at the center of the trap as a function of U . For a given value of U , the inhomogeneous system can be represented by a vertical line originating at μ_0 .

to the homogeneous case, (2) kinks develop over a certain range of U and (3) the visibility drops drastically for particular values of U and for further increase in U , the variation is slow. Similar behavior is also noted in the condensate fraction.

For a given value of U and number of bosons N , the homogeneous system represents a point (μ, U) in the phase diagram given in the Fig. (6). However, for an inhomogeneous system the chemical potential varies across the lattice and is represented by a vertical line (see Fig. (12)), originating at μ_0 for a given U in the $(\mu-U)$ plane, where μ_0 is the chemical potential at the center of the trap. The values of μ_0 as a function of U is shown in Fig. (12). The behavior of the condensate fraction and visibility (shown in Figs. (10) and (11)) is then easily understood by trac-

ing the μ_0 trajectory as a function of U . For $U < 6.0$, a vertical line starting at μ_0 , representing possible values of the local chemical potential for a given U , does not intersect the MI lobe and no Mott plateau forms in the density profile. As U increases, the system begins to favor the MI phase, and as a result the condensate fraction and the visibility decreases monotonically. However, for $U > 6.0$, the vertical line, intersects the Mott lobe, resulting in a well-developed Mott plateau in the density profile. All the kinks in the condensate fraction and the visibility are observed for $U > 6.0$, indicating the formation and broadening of the Mott plateau in the system, as the bosons re-distribute themselves between the two phases across the lattice. Finally for larger values of U , the μ_0 trajectory enters the Mott lobe and the central SF region vanishes completely. The entire system is in the Mott phase except for the edges. As a result, the condensate fraction and the visibility drops drastically. Further increase in U results in smooth variations of both these quantities as the SF phases exist only at the edges and the number of bosons in the SF phases do not vary much as shown in Fig. (8).

In the experiments, the chemical potential is usually changed by changing the number of bosons N . We plot, in Fig. (13), the variation of the condensate fraction and the visibility as a function of N , for $V_t = 0.008$ and $U = 10$. We see that when the MI plateau forms, both visibility and condensate fraction dip, the first of these corresponding to the formation of a $\rho = 1$ Mott plateau, occurs around $N \sim 40$. This can be observed in the density profile (see Fig. (14)). The plateau in Fig. (13), in the condensate fraction, indicates the range of N for which the $\rho = 1$ MI phase is possible for the given U value. We note that beyond $N \sim 56$, a $1 \leq \rho \leq 2$ SF forms, marked by an increase in the visibility and the condensate fraction. The second minimum occurs around $N \sim 140$ signals the formation of the second Mott plateau ($\rho = 2$), as shown in Fig. (14). Further increase in N , beyond $N \sim 150$, results in another SF phase, with the on-site density ranging between $2 \leq \rho \leq 3$. Therefore, for a fixed value of U , the minima in the condensate fraction and the visibility as a function of N are good indicators for the formation of Mott plateaus.

V. CONCLUSION

This paper demonstrates a way of extracting the phase diagram for the Bose-Hubbard model in the presence of an external trapping potential, from the number density profile. Signatures of these phases in experimentally observed quantities such as visibility, condensate fraction and $N(\rho)$ have been documented. We have also obtained the density-profile as a function of the chemical potential for the homogeneous case, using FS-DMRG for the first time, to the best of our knowledge.

Future directions are immense. As a first step, the extended Bose-Hubbard model can be investigated and

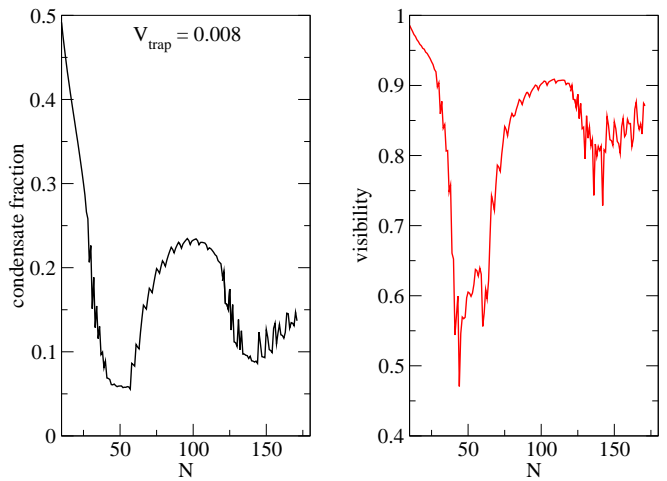


FIG. 13: Condensate fraction (left) and visibility (right) as a function of N the total number of bosons in a trap of depth $V_t = 0.008$ and $U = 10$. Both the condensate fraction and visibility show local minima for particular ranges of N , indicating the formation of MI phases. The subsequent increase in these quantities indicate the formation of SF phases.

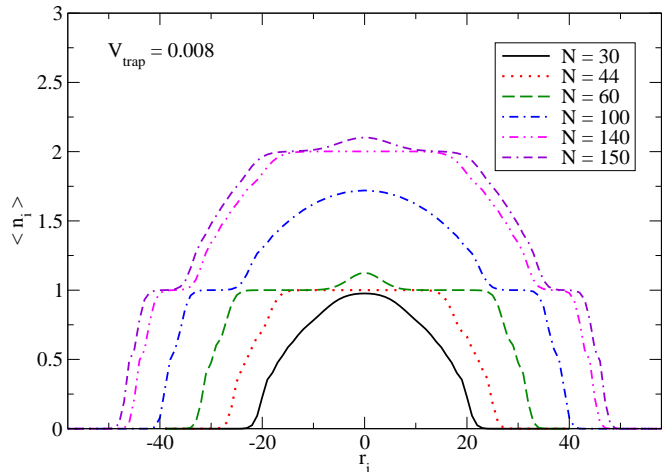


FIG. 14: Density profile for different total number of bosons N . Note that the minima in visibility and condensate fraction in Fig. (13) correspond to formation of MI plateaus.

the phase diagram, together with the experimental signatures for the various phases can be extracted in an analogous way, which is in progress. The influence of a three-body term for the Bose-Hubbard and the extended Bose-Hubbard can be investigated, which is also in progress.

The presence of a trap makes the system interesting due to the simultaneous existence of different phases (such as the SF and the MI phase in this work) and gets the theoretical predictions closer to experiments. It would also be interesting to study the Bose-Hubbard model for two boson species and Bose-Fermi mixtures in the presence of a trap. This paper serves more as benchmark to extract the phase diagram in a straight-forward

and transparent way from the density profile. This technique can now be extended to other problems.

Acknowledgments

The computations were carried out on the Garuda grid

and we thank its members for their support. ML thanks the Indian Institute of Astrophysics, Bangalore for their hospitality, where all of this work was carried out. RVP thanks CSIR, India Grant No. 03(1107)/08/EMR-II.

-
- [1] F. Dalfovo, S. Giorgini, L. P. Pitaevskii and S. Stringari, *Rev. Mod. Phys.* **71** 463 (1999).
- [2] I. Bloch, J. Dalibard, and W. Zwerger, *Rev. Mod. Phys.* **80** 885 (2008).
- [3] M. Lewenstein, A. Sanpera, V. Ahufinger, B. Damski, A. Sen and U. Sen, *Advances in Physics*, **56** 243 (2007).
- [4] M.P.A. Fisher, P.B. Weichmann, G. Grinstein and D.S. Fisher, *Phys. Rev. B* **40**, 546 (1989).
- [5] W. Krauth, M. Caffarel, and J. P. Bouchaud, *Phys. Rev. B* **45**, 3137 (1992).
- [6] K. Sheshadri, H. R. Krishnamurthy, R. Pandit, and T. V. Ramakrishnan, *Europhys. Lett.* **22**, 257 (1993).
- [7] L. Amico and V. Penna, *Phys. Rev. Lett.* **80**, 2189 (1998).
- [8] T. D. Kuhner and H. Monien, *Phys. Rev. B* **58**, R14741 (1998); T.D. Kuhner, S.R. White, H. Monien, *Phys. Rev. B*, **61**, 12474 (2000).
- [9] R. V. Pai and R. Pandit, *Phys. Rev. B* **71**, 104508 (2005).
- [10] R.V.Pai, R.Pandit, H.R. Krishnamurthy and S. Ramasesha, *Phys. Rev. Lett.* **76**, 2937 (1996).
- [11] V. A. Kashurnikov and B. V. Svistunov, *Phys. Rev. B* **53**, 11776 (1996).
- [12] G. G. Batrouni, R. T. Scalettar, G. T. Zimanyi, and A. P. Kampf, *Phys. Rev. Lett.* **74**, 2527 (1995); P. Niyaz, R. T. Scalettar, C. Y. Fong, and G. G. Batrouni, *Phys. Rev. B* **44**, 7143 (1991).
- [13] J.K. Freericks and H. Monien, *Europhys. Lett.* **26**, 2691 (1994); J.K. Freericks and H. Monien, *Phys. Rev. B* **53**, 2691 (1996).
- [14] B. Capogrosso-Sansone, N. V. Prokofev, and B. V. Svistunov, *Phys. Rev. B* **75**, 134302 (2007).
- [15] Barbara Capogrosso-Sansone, Sebnem Gunes Soyler, Nikolay Prokof'ev and Boris Svistunov, arXiv:0710.2703 [cond-mat.other]
- [16] D. Jaksch, C. Bruder, J. I. Cirac, C. W. Gardiner, and P. Zoller, *Phys. Rev. Lett.* **81**, 3108 (1998).
- [17] M. Greiner, O. Mandel, T. Esslinger, T. W. Haensch, and I. Bloch, *Nature* **415**, 39 (2002).
- [18] I. B. Spielman, W. D. Phillips, and J. V. Porto, *Phys. Rev. Lett.* **98** 080404 (2007).
- [19] T. Stoferle, H. Moritz, C. Schori, M. Koehl, and T. Esslinger, *Phys. Rev. Lett.* **92**, 130403 (2004).
- [20] S. Wessel, F. Alet, M. Troyer and G. G. Batrouni, *Phys. Rev. A*, **70** 053615 (2004).
- [21] V. A. Kashurnikov, N. V. Prokofev, and B. V. Svistunov, *Phys. Rev. A*, **66**, 031601 (2002).
- [22] D. van Oosten, P. van der Straten, and H. T. Stoof, *Phys. Rev. A* **63** 053601 (2001).
- [23] S. Bergkvist, P. Henelius, and A. Rosengren, *Phys. Rev. A* **70**, 053601 (2004).
- [24] Lode Pollet, Stefan Rombouts, Kris Heyde, and Jorge Dukelsky, *Phys. Rev. A* **69**, 043601 (2004).
- [25] B. DeMarco, C. Lannert, S. Vishveshwara, and T.-C. Wei, *Phys. Rev. A* **71**, 063601 (2005).
- [26] Kaushik Mitra, C. J. Williams, C. A. R. Sa de Melo, *Phys. Rev. A* **77**, 033607 (2008).
- [27] Simon Fölling, Artur Widera, Torben Müller, Fabrice Gerbier, and Immanuel Bloch, *Phys. Rev. Lett.* **97**, 060403 (2006).
- [28] G. K. Campbell, J. Mun, M. Boyd, P. Medley, A. E. Leanhardt, L. G. Marcassa, D. E. Pritchard, W. Ketterle, *Science* **313**, 649 (2006).
- [29] Fabrice Gerbier, Artur Widera, Simon Fölling, Olaf Mandel, Tatjana Gericke and Immanuel Bloch, *PRA* **72**, 053606, (2005).
- [30] Kosterlitz J M and Thouless D. J., *J. Phys.* **C6** 1181, (1973).
- [31] Thierry Giamarchi, *Quantum Physics in One Dimension*, Clarendon Press, Oxford, (2004).
- [32] G. G. Batrouni et. al. *Phys. Rev. Lett.* **89**, 117203 (2002)
- [33] C. Kollath, U. Schollwöck, J. von Delft, W. Zwerger, *Phys. Rev. A* **71** **69** (Rapid Communication), 031601 (2004).
- [34] Laura Urba *et al* *J. Phys. B: At. Mol. Opt. Phys.* **39** 5187 (2006).
- [35] G.G. Batrouni, H. R. Krishnamurthy, K. W. Mahmud, V.G. Rousseau, R.T. Scalettar *Phys. Rev. A* **78**, 023627 (2008).
- [36] S. R. White, *Phys. Rev. Lett.* **69**, 2863 (1992); *Phys. Rev. B* **48**, 10345 (1993).
- [37] U. Schollwöck, *Rev. Mod. Phys.* **77**, 259 (2005).
- [38] P. Sengupta, M. Rigol, G. G. Batrouni, P. J. H. Denteneer and R. T. Scalettar, *Phys. Rev. Letts.* **95**, 220402, (2005).
- [39] R. B. Diener, Q. Zhou, H. Zhai and Tin-Lin Ho, *Phys. Rev. Lett.* **98**, 180404 (2007) arXiv:cond-mat/0609685
- [40] Y. Kato, Q. Zhou, N. Kawashima and N. Trivedi, *Nature Physics* **4**, 617, (2008).
- [41] F. Gerbier, A. Widera, S. Fölling, O. Mandel, T. Gericke and I. Bloch, *Phys. Rev. Letts.* **95**, 050404 (2005).
- [42] A. J. Leggett, *Rev. of Mod. Phys.*, **73** (2001).